Picosecond laser action on iron films: elastic, plastic and polymorphic transformations

Khokhlov V A (1)**, Ashitkov S I** (2)**, Inogamov N A** (1,3,2)**, Komarov P S** (2)**, Mursov S A** (3,1)**, Struleva E V** (2) **and Zhakhovsky V V** (3,2,1)

(1) Landau Institute for Theoretical Physics of the Russian Academy of Sciences, Akademika Semenova 1a, Chernogolovka, Moscow Region 142432, Russia

(2) Joint Institute for High Temperatures of the Russian Academy of Sciences, Izhorskaya 13 Bldg 2, Moscow 125412, Russia

(3) Dukhov Research Institute of Automatics (VNIIA), Sushchevskaya 22, Moscow 127055, Russia

v_a_kh@mail.ru,

http://laser.itp.ac.ru/

The use of high-power nanosecond lasers for studying the equations of state of condensed matter:
S. I. Anisimov, A. M. Prokhorov and V. E. Fortov, 1982, Bull. Ac. Sci. USSR, Phys. Ser. **46,** 63–69
S. I. Anisimov, A. M. Prokhorov and V. E. Fortov, 1984, Sov. Phys. Usp. **27,** 181–205
Ya. B. Zel'dovich and Yu. P. Raiser, 1967, Physics of shock waves and high-temperature hydrodynamic phenomena (N.-Y.: Academic Press)

Solid phases of iron (α (bcc—body-centered cubic lattice), γ (fcc—face-centered cubic), δ (bcc) and ε (hcp—hexagonal close-packed))
G. I. Kerley, 1993, Preprint SAND93-0027 (Sandia National Laboratories)

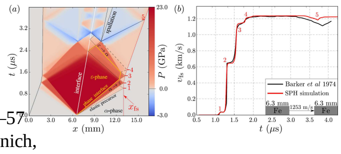

Phase transition $\alpha \rightarrow \varepsilon$ in iron in shock-wave experiments (three-shock wave configuration)
L. M. Barker and R. E. Hollenbach, 1974, J. Appl. Phys. **45,** 4872
G. E. Duvall and R. A. Graham, 1977, Rev. Mod. Phys. **49,** 523
A. V. Ananyin, A. N. Dremin and G. I. Kanel', 1981, Physics of combustion and explosion, No 3, 93–102
V. D. Gluzman, G. I. Kanel', V. F. Loskutov, V. E. Fortov and E. I. Horev, 1985 Problems of strength, No 8, 52–57
J. C. Crowhurst, B. W. Reed, M. R. Armstrong, H. B. Radousky, J. A. Carter, D. C. Swift, J. M. Zaug, R. W. Minich, N. E. Teslich and M. Kumar, 2014, J. Appl. Phys. **115,** 113506 - *possibility of polymorphic $\alpha \rightarrow \varepsilon$ transformations in times more then 100 ps at pressures above 25 GPa, which is approximately 2 times higher than under microsecond loading.*

Superelastivity (sharp increase in the threshold separating elastic and plastic shockwave)
S. I. Ashitkov, M. B. Agranat, G. I. Kanel', P. S. Komarov and V. E. Fortov, 2010, JETP Lett. **92,** 516–520
V. H. Whitley, S. D. McGrane, D. E. Eakins, C. A. Bolme, D. S. Moore and J. F. Bingert, 2011, J. Appl. Phys. **109,** 013505
J. C. Crowhurst, M. R. Armstrong, K. B. Knight, J. M. Zaug and E. M. Behymer, 2011, Phys. Rev. Lett., **107,** 144302
R. F. Smith, J. H. Eggert, R. E. Rudd, D. C. Swift, C. A. Bolme and G. W. Collins, 2011, J. Appl. Phys., **110,** 123515
G. I. Kanel', 2012, AIP Conf. Proc., **1426,** 939
V. V. Zhakhovskii and N. A. Inogamov, 2010, JETP Lett., **92,** 521–526
V. V. Zhakhovsky, M. M. Budzevich, N. A. Inogamov, I. I. Oleynik and C. T. White, 2011, Phys. Rev. Lett., **107,** 135502
N. A. Inogamov, V. V. Zhakhovskii, V. A. Khokhlov and V. V. Shepelev, 2011, JETP Lett., **93,** 226–232
B. J. Demaske, V. V. Zhakhovsky, N. A. Inogamov and I. I. Oleynik, 2013, Phys. Rev. B, **87,** 054109
V. V. Zhakhovsky, N. A. Inogamov, B. J. Demaske, I. I. Oleynik and C. T. White, 2014, J. Phys.:Conf. Ser., **500,** 172007
R. Perriot, V. V. Zhakhovsky, N. A. Inogamov and I. I. Oleynik, 2014 J. Phys.: Conf. Ser. **500** 172008

First, I want to remember Vladimir Evgenievich Fortov and Gennady Isakovich Kanel.
Under the action of pulses in the microsecond range at the a-e transition, a characteristic three-shock configuraton is observed.
In the picosecond range, such a three-wave configuration is not observed.
We have already encountered a similar situation in the study of elastic-plastic shock waves, when the pressure in the wave can significantly exceed the classical elastic limit, but it moves as elastic.

Experimental scheme. Ultrafast spectral interferometry

The experimental samples were Armco iron films 580, 740, 970, and 1160 nm thick, deposited by the magnetron method on glass substrates 150 µm thick.

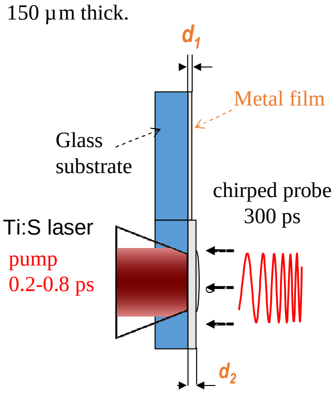

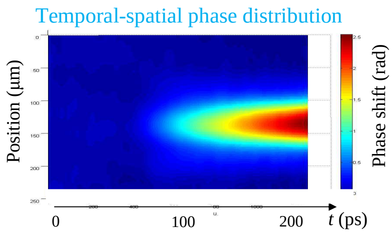

$$\Delta z(y,t) = \lambda(t)\Delta\varphi(y,t)/4\pi$$

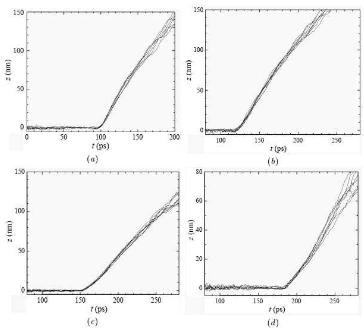

Displacement histories of the free surface of iron samples with thickness: (a)—580 nm, (b)—740 nm, (c)—970 nm, (d)—1160 nm

Lagrange inverse analysis of kinematic data

Stress and strain are directly
integrated from conservation laws

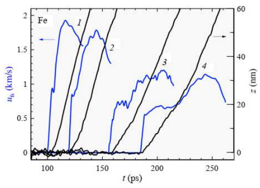

Wave profiles of displacement (black lines) and velocity (blue lines) of the free surface of iron film samples with thickness: 1—580 nm, 2—740 nm, 3—970 nm, 4—1160 nm

$$\frac{\partial \sigma}{\partial h} = -\rho_0 \frac{\partial u}{\partial t} \qquad \sigma = -p_{xx}$$

$$\frac{\partial \mu}{\partial t} = -\frac{\partial u}{\partial h} \qquad \mu = 1 - V / V_0$$

$$\rho_0 = 7.874 \text{ g/cm}^3$$

Inferring experimental profiles $u_{fs} = 2u$ with different width *h*, defines $u = u(t, h)$

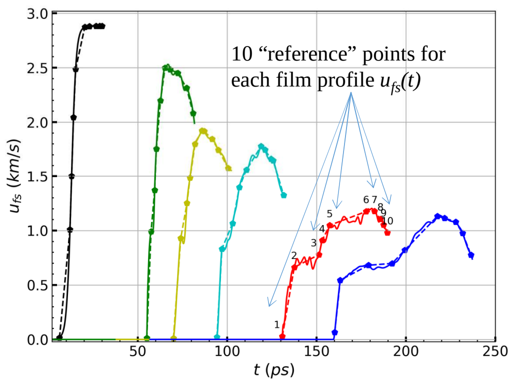

John B. Aidun *and* Y. M. Gupta Analysis of Lagrangian gauge measurements of simple and nonsimple plane waves Journal of Applied Physics 69, 6998 (1991)

4

Lagrange inverse analysis method was successfully used for inferring experimental results.
The main idea is Lagrangian form of mass and momentum equations where right hand side depend on u(t,h) and parameter of initial density. Therefore if our experimental data could be approximated as a function of two variable h (Lagrange coordinate) and t (time), we may directly integrate it for calculating stress and strain.

Though we have six films with a precise history of free surface velocity, which is doubled mass velocity for each fixed Lagrangian coordinate h.

The function u(t,h) is approximated with linear piecewice interpolation using 10 reference points at each profile.

Stress-Strain diagram inferred from kinematic data

$$\sigma(t,h) = -\rho_0 \int_{h_b}^{h} \frac{\partial u}{\partial t}(t,h_1)\,dh_1 \qquad \mathrm{V}(t,h)/\mathrm{V}_0 = 1 - \int_{t_b}^{t} \frac{\partial u}{\partial h}(t_1,h)\,dt_1.$$

The ε - phase occurs not in the jump, but in the unloading wave!

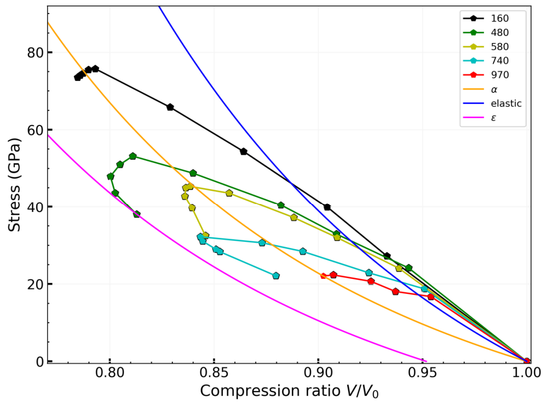

*Poster session March 2 for details. Murzov S.A., Inogamov N.A., Zhakhovsky V.V., Khokhlov V.A., Ashitkov S.I., Struleva E.V., Romashevsky P.S., *Shock-induced elastic, plastic and polymorphic transformations in iron films by picosecond laser pulse.*

5

Then stress and strain are integrated and state diagram could be obtained for all except the largest width 1160 nm, because we use only interpolated data.
There are three shock Hugoniots are shown for elastic, alpha and epsilon-phase iron. And five paths for different films width. It was surprisingly observed, that transition to epsilon phase appeared in the unloading part of profiles. That is peculiarity of ultra-short impulse response we suppose.

Numerical simulations.

Two-temperature hydrodynamics

$$
\begin{aligned}
\frac{\partial x(x^0,t)}{\partial t} &= v(x^0,t),\\
\rho\,\frac{\partial x(x^0,t)}{\partial x^0} &= \rho_0,\\
\frac{\partial v(x^0,t)}{\partial t} &= -\frac{1}{\rho^0}\frac{\partial P(x^0,t)}{\partial x^0}, \qquad P = P_\mathrm{e} + P_\mathrm{i},\\
\frac{\partial E_\mathrm{e}(x^0,t)}{\partial t} &= \frac{1}{\rho^0}\frac{\partial}{\partial x^0}\left(\frac{\kappa_\mathrm{e}\rho}{\rho^0}\,\frac{\partial T_\mathrm{e}}{\partial x^0}\right) - \alpha_\rho(T_\mathrm{e}-T_\mathrm{i}) + \frac{Q(x^0,t)}{\rho} - \frac{P_\mathrm{e}}{\rho_0}\,\frac{\partial v}{\partial x^0},\\
\frac{\partial E_\mathrm{i}(x^0,t)}{\partial t} &= \frac{1}{\rho^0}\frac{\partial}{\partial x^0}\left(\frac{\kappa_\mathrm{i}\rho}{\rho^0}\,\frac{\partial T_\mathrm{i}}{\partial x^0}\right) + \alpha_\rho(T_\mathrm{e}-T_\mathrm{i}) - \frac{P_\mathrm{i}}{\rho^0}\,\frac{\partial v}{\partial x^0},
\end{aligned}
$$

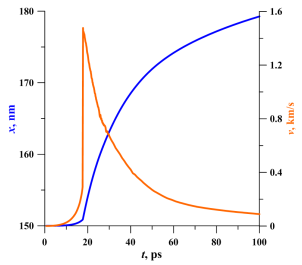

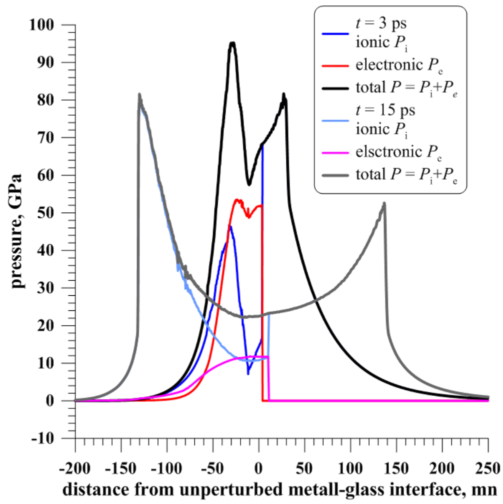

In metal for the electronic component, we use analytical approximations based on DFT-calculations.
For the ionic component, a tabular wide range equation of state is used, which takes into account the gas, liquid and solid alpha phases, calculated by K. Khishchenko
In glass, which is always assumed to be solid, it.s own analytic equation of state of the Mie-Grüneisen type is used, own initial density.
There is no electronic component in the glass.

MD simulation of SW in polycrystalline iron

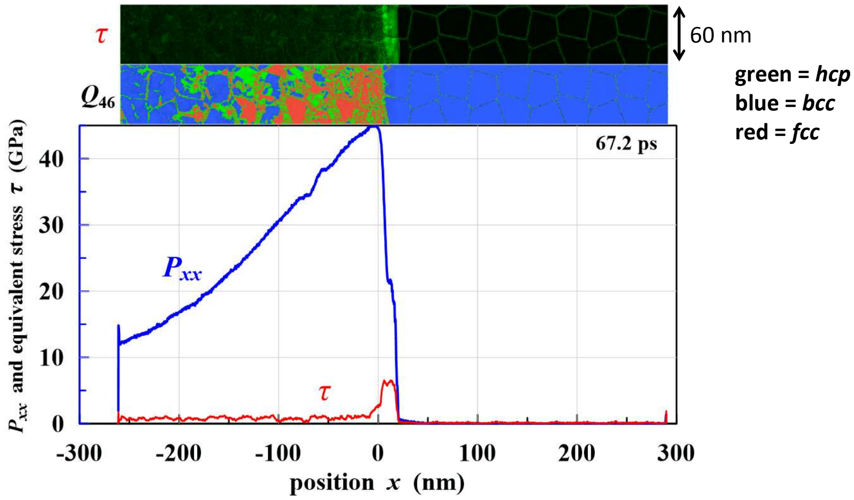

Left piston moves with the velocity of Lagrangian particle taken from 2T-HD modeling. Sample dimensions 590x60x10 nm. Grain boundaries are perpendicular to xy-plane.

There is piston on the left, that moves in according with results of hydrodynamic calculations (Lagrange node x^0 = -150 nm)

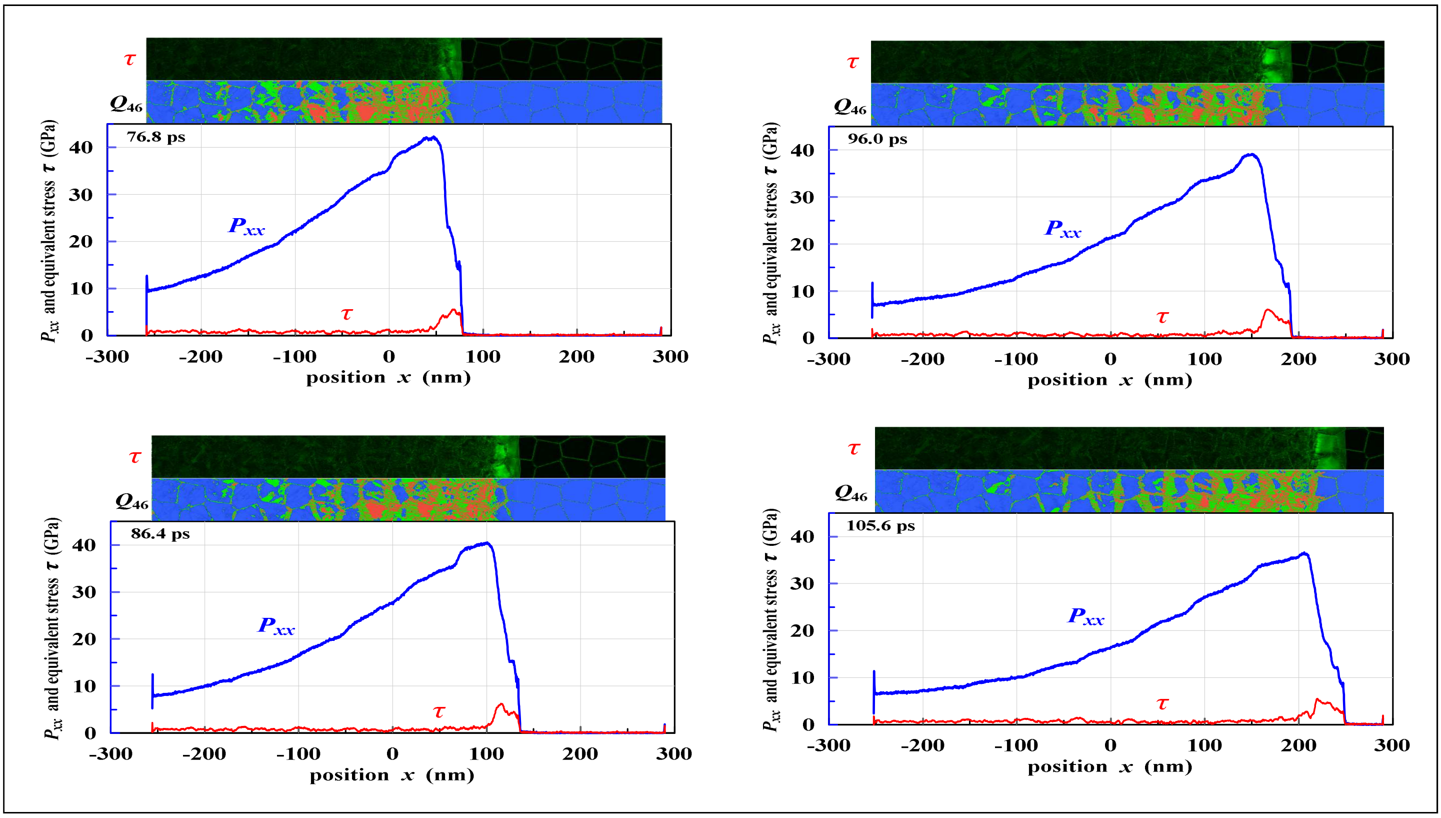

На этом слайде отдельные картинки.

Размер исходного образца 590х60х10 нм. Образец состоит из ~30 миллионов атомов.
Время в левом углу указано с начала истории лагранжевой частицы (т.е. с t=0 в 2Т коде).
Ориентация крист.решетки в зернах случайная.

Грани всех зерен строго перпендикулярны экрану (плоскости ху).
Это позволяет строить карты величин усредненных на всю глубину Z (=10 нм)

Validation of Lagrange inverse analysis by MD simulation of polycrystalline iron: 2

Lagrange particles histories form MD → **Reconstructed stress-strain curves**

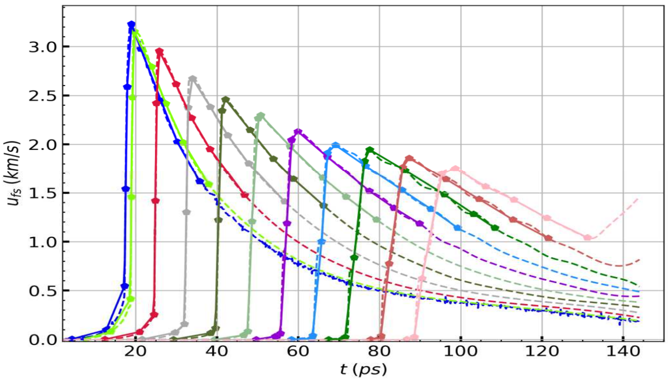

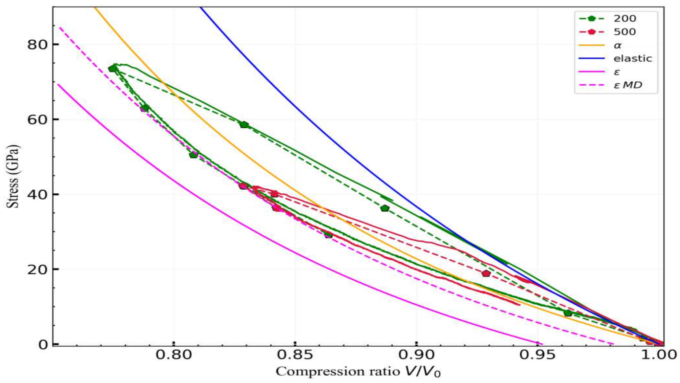

- MD simulation provides full information about selected Lagrange particles.
- 11 particles with h=150, 200, …600 and 160 nm are used.
- Solid P-V lines from the inverse analysis, Dashed P-V lines from MD.

Для валидации метода используется запись истории состояния лагранжевых частиц из молекулярно-динамического моделирования. Набор профилей частиц с координатой h от 150 до 600 нм показан на рисунке слева. В результате восстановлена диаграмма путей состояния продольного напряжения-деформации и показана для частиц с h=200 и 500 нм. На правом графике показаны снова адиабаты железа для упругой и альфа-эпсилон фаз, причем эпсилон фаза железа, наблюдаемая в МД моделировании показана пунктиром. Наблюдается хорошее согласие диаграммы из МД моделирования и рассчитанной при восстановлении.

For validation of the inverse analysis technique the molecular dynamics histories of Lagrange particles are recorded. A series of these recorded free surface velocity profiles with particles initial positions from 150 to 600 nm are shown on the left figure. The stress-strain diagram is inferred and shown for Lagrange particles h=200 and 500 nm. On the right, shock Hugoniots of iron in elastic, alpha and epsilon phases are shown. Epsilon phase Hugoniot for iron from MD simulation is shown with dashed line. A good agreement of the inverse analysis and the molecular dynamics is observed.

Conclusions

This paper presents the results of experiments with laser shock waves in iron films. It is known that iron has an alpha-epsilon phase transition. Upon transition, the crystal rearranges its lattice from body-centered cubic (bcc) to hexagonal close-packed (hcp). The transition occurs under a quasi-stationary load with an increase in pressure above 13 GPa. The transition is observed both under stationary conditions (for example, diamond anvils) and under quasi-stationary conditions. Such quasi-stationary conditions include loads in shock waves propagating in the order of millimeter thick targets.

The analysis of the experimental data (these are the dependences of the speed of the free rear surface on time) was carried out by two methods. This analysis makes it possible to determine the profiles of density and longitudinal stress from the experimental data. Further, these profiles are projected onto the phase plane: inverse compression ratio—longitudinal stress. The first method allows you to reach only the state behind the front of the 2nd jump. Whereas the second method describes both jumps and the unloading wave behind them. The methods are in good agreement in the section of the first (elastic) and second (plastic) shock waves

We note that in experiments in the submicrosecond loading range, a three-wave configuration of elastic, plastic waves and a jump of the $\alpha \rightarrow \varepsilon$ transition is observed. In our experiments with ultrafast loading, we do not see the third jump. It is striking that the approach to the epsilon phase occurs not in the jump, but in the unloading wave.

Thank you for your attention

Experimental scheme

Chirped pulse with linear frequency modulation with a duration of about 300 ps with a spectral width of 40 nm and a central wavelength λ0 = 795 nm

The source of heating and diagnostic pulses was a titanium—sapphire laser system,
the duration of the heating pulse was 1.2 ps.
The laser pulse energy was E = 100 ± 5 mJ, which corresponds to the incident energy density F_0 at the center of the focal spot about 3.4 J/cm^2.

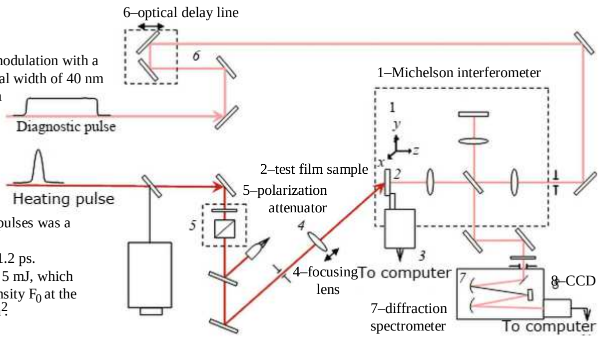

The experimental samples were Armco iron films 580, 740, 970, and 1160 nm thick, deposited by the magnetron method on glass substrates 150 µm thick.

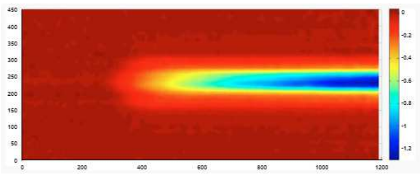

$$\Delta z = \lambda \Delta\varphi / 4\pi.$$

Spatio-temporal distribution of the phase of the diagnostic pulse when the shock wave reaches the free surface.
Time scan is vertical scale in microns. The cross section along the short axis of the ellipse is the horizon scale in ps.

Experimental results

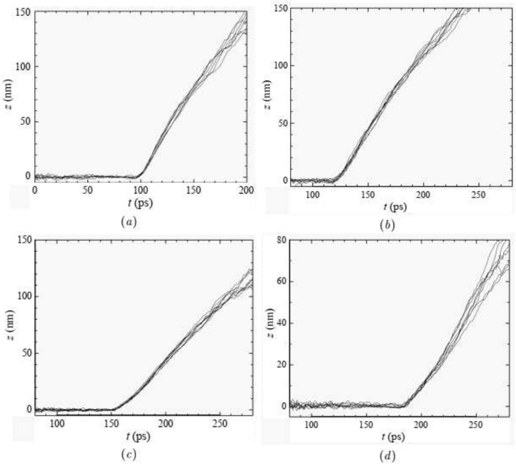

Displacement histories of the free surface of iron samples with thickness:
(a)—580 nm, (b)—740 nm, (c)—970 nm, (d)—1160 nm

Experimental results.
The evolution of the shock wave

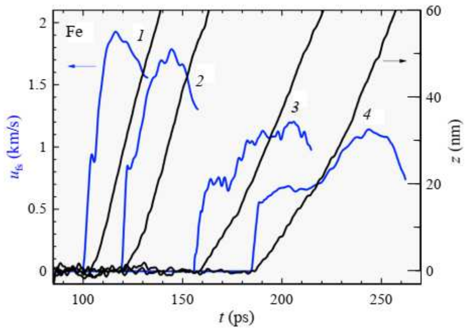

Wave profiles of displacement (black lines) and velocity (blue lines) of the free surface of iron film samples with thickness:
1—580 nm, 2—740 nm, 3—970 nm, 4—1160 nm

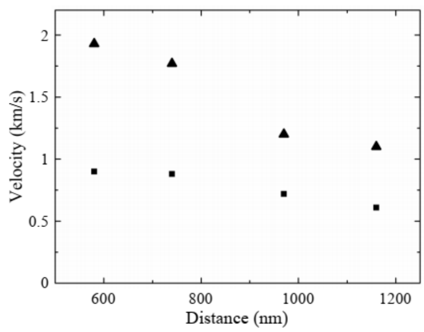

Attenuation of elastic (squares) and plastic (triangles) waves at a propagation length from 580 nm to 1160 nm in iron.

Experimental results.

The evolution of the shock wave

h, nm	t^{el}, ps	u_{HEL}, km/s	u_p, km/s	V/V_0	σ_{HEL}, GPa
580	96.5	0.90	0.45	0.932	23.5
740	120.3	0.88	0.44	0.934	22.9
970	154.3	0.72	0.36	0.945	18.4
1160	184.5	0.61	0.305	0.953	15.4

Values of the exit time t^{el} , the velocity of the free surface u_{HEL} and mass velocity u_p, degree of shock compression V/V_0 and stress values σ_{HEL} behind the elastic precursor front for specimens of thickness h according to experimental data

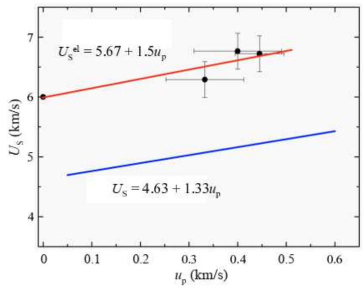

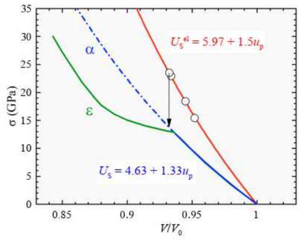

$\sigma_{HEL} = \rho_0 U_S u_{HEL}/2$

$V/V_0 = 1 - u_p/(c_l + bu_p),$

$\sigma_{HEL} = \rho_0 c_l^2 (1 - V/V_0)/[1 - b(1 - V/V_0)]^2$

Comparison of the results of measurements of the shock wave velocity U_S and the mass velocity behind its front u_p (markers) with elastic (red line) and plastic (blue line) iron shock adiabates

Experimental results and
Inverse analysis of kinematic data

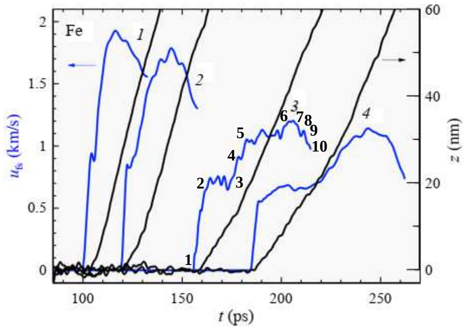

Wave profiles of displacement (black lines) and velocity (blue lines) of the free surface of iron film samples with thickness:
1—580 nm, 2—740 nm, 3—970 nm, 4—1160 nm
Points 1—10 are the nodes of the polyline that approximates the velocity dependence.

Calculation of normal stress $\sigma = -p_{xx}$ and strain ϵ

$$\frac{\partial \sigma}{\partial h} = -\rho_0 \frac{\partial u}{\partial t}$$

$$\frac{\partial \epsilon}{\partial t} = -\frac{\partial u}{\partial h}$$

$$\sigma(t_1, h_1) - \sigma(t_1, h_b) = -\rho_0 \int_{h_b}^{h_1} \frac{\partial u}{\partial t}(h, t_1) dh$$

$$\epsilon(t_1, h_1) - \epsilon(t_b, h_1) = -\int_{t_b}^{t_1} \frac{\partial u}{\partial h}(h_1, t) dt$$

Calculations in the piecewise quasi-stationary approximation (PQsA)

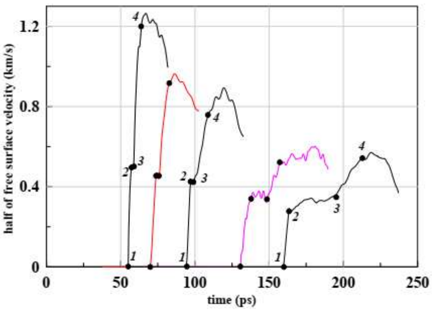

Free surface velocity profiles for thick films from left to right: 160, 480, 580, 740, 970 and 1160 nm. Points *1–2* and *3–4* indicate elastic and plastic waves, respectively.

Using the law of conservation of mass on the elastic section *1–2*,

$\rho = \rho_0 U_s|_e / (U_s|_e - u)$ $U_s|_e$ is the elastic jump velocity

The longitudinal component of the stress increases with the velocity u according to the law

$$\sigma = \sigma_0 + \rho_0 (U_s|_e)^2 - \rho (U_s|_e - u)^2.$$

$$\sigma = \rho_0 (U_s|_e) u.$$

The stress in the film before the arrival of the wave, $\sigma_0 = 0$

On a homogeneous area *2–3*, the density and stress are

$$\rho_{23} = \rho_0 U_s|_e / (U_s|_e - u_2),$$

$$\sigma_{23} = \rho_0 (U_s|_e) u_2.$$

In the same way, on plastic section *3–4* $\rho = \rho_{23} \dfrac{U_s|_p - u_2}{U_s|_p - u}.$

$$\sigma + \rho (U_s|_p - u)^2 = \sigma_{23} + \rho_{23} (U_s|_p - u_2)^2.$$

$$\sigma = \sigma_{23} + \rho_{23} (U_s|_p - u_2)(u - u_2).$$

Calculations in the piecewise quasi-stationary approximation (PQsA)

160 nm thick film

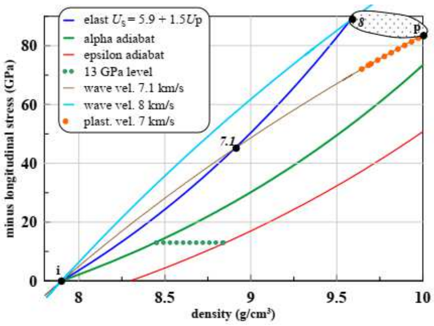

Iron phase plane. The adiabats are shown: elastic compression in the approximation of an isotropic elastic body (blue curve, elast), the adiabats of the α and ε phases—green and red curves, respectively. Along with the adiabats, the profiles for the 160 nm film are presented. The blue and brown profiles are obtained at wave propagation speeds of 8 and 7.1 km/s. The velocity 7.1 corresponds to the average wave velocity over the 480–160 nm range of propagation distances.

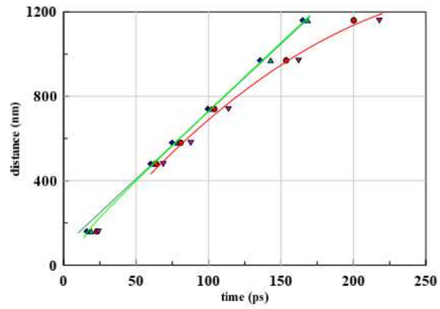

Plastic wave trajectory plotted together with elastic wave trajectory. The pair of markers and curves of blue and green shades refer to wave
1–2. The pair of red shade markers and the red curve represent plastic wave 3–4 data.
The approximations of experimental data (markers) are given by solid curves.

Calculations in the piecewise quasi-stationary approximation (PQsA)
480 and 740 nm thick films

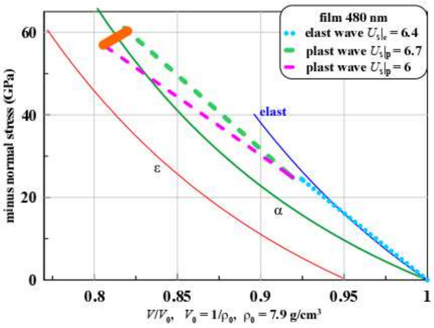

Three adiabats and profiles for plastic wave velocities *U*s|p = 6 and 6.7 km/s are presented. The bold orange segment outlines the geometric position of the points *4* (the end point of the plastic wave) on the given phase plane at a speed variation of *U*s|p in the range from 6 to 6.7 km/s.

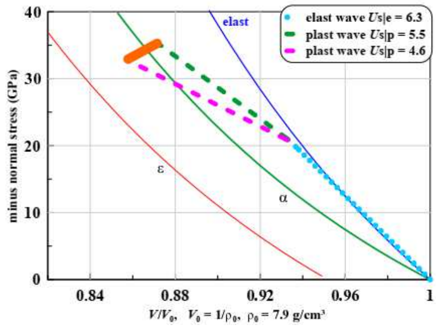

Three adiabats and profiles for the velocities of elastic and plastic waves at the exit from a 740 nm film are presented. The bold orange segment is the position of points 4 in figure 11 for a given film on the phase plane. The segment is filled with velocity variation Us|p in the range from 5.5 to 4.6 km/s

Calculations in the piecewise quasi-stationary approximation (PQsA)

970 and 1160 nm thick films

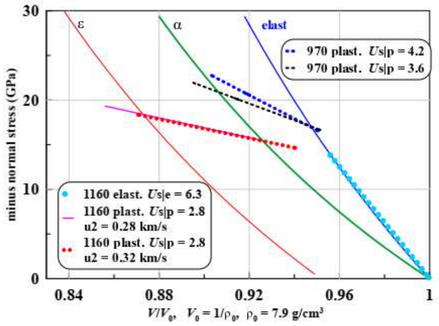

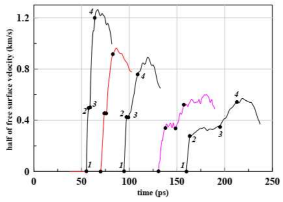

Repetition of adiabats and profiles for 970 and 1160 nm films. The numbers 970 and 1160 in the picture field indicate the thickness of the films. The rest of the numbers give the speed in km/s.

Calculations in the piecewise quasi-stationary approximation (PQsA)

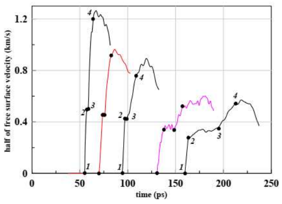

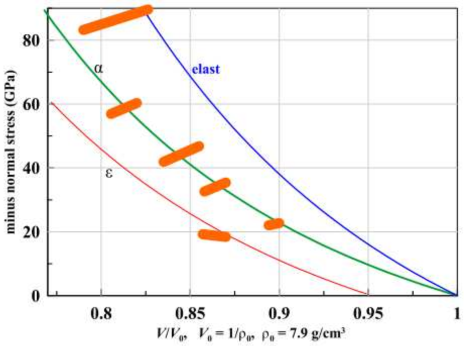

A generalization of calculations by the piecewise quasi-stationary approximation method for all six films is shown. The six orange areas show the states behind the waves *1–2* and *3–4* on the phase plane. From top to bottom, there are thicknesses from 160 nm to 1160 nm: 160, 480, 580, 740, 970 and 1160 nm. According to the PQsA, the fraction of the ε-phase is small in the mixture of α and ε-phases. The only exception is the lowest region, which belongs to the 1160 nm film. In it, according to the PQsA, a complete transition to the ε-phase occurs.